J Mol Model (2013) 19:4319–4335
DOI 10.1007/s00894-013-1948-z

ORIGINAL PAPER

Self-assembly of cationic surfactants on the carbon nanotube surface: insights from molecular dynamics simulations

Niaz Poorgholami-Bejarpasi · Beheshteh Sohrabi

Received: 15 April 2013 / Accepted: 12 July 2013 / Published online: 1 August 2013

Abstract The insolubility of carbon nanotubes (CNTs) in aqueous media has been a limitation for the practical application of this unique material. Recent studies have demonstrated that the suspend ability of CNT can be substantially improved by employing appropriate surfactants. Although various surfactants have been tested, the exact mechanism by which carbon nanotubes and the different surfactants interact is not fully understood. To deepen the understanding of molecular interaction between CNT and surfactants, as well as to investigate the influence of the surfactant tail length on the adsorption process, we report here the first detailed large-scale all-atomistic molecular dynamics simulation study of the adsorption and morphology of aggregates of the cationic surfactants containing trimethylammonium headgroups (C_{12}TAB and C_{16}TAB) on single-walled carbon nanotube (SWNT) surfaces. We find that the aggregation morphology of both C_{12}TAB and C_{16}TAB on the SWNT is dependent upon the number of the surfactants in the simulation box. As the number of the surfactants increases the random monolayer structure gradually changes to the cylinder-like monolayer structure. Moreover, we make a comparison between the C_{12}TAB and C_{16}TAB adsorption onto SWNTs to clarify the role of the surfactant tail length on the adsorption process. This comparison indicates that by increasing the number of surfactant molecules, the larger number of the C_{16}TAB molecules tend to adsorb onto SWNTs. Further, our results show that a longer chain yields the higher packed aggregates in which the surfactant heads are extended far into the aqueous phase, which in turn may increase the SWNTs stabilization in aqueous suspensions.

Keywords Carbon nanotube · Cationic surfactants · Molecular dynamics simulations · Tail length

Electronic supplementary material The online version of this article (doi:10.1007/s00894-013-1948-z) contains supplementary material, which is available to authorized users.

N. Poorgholami-Bejarpasi · B. Sohrabi (✉)
Department of Chemistry, Surface Chemistry Research Laboratory, Iran University of Science and Technology, P.O. Box 16846-13114, Tehran, Iran
e-mail: Sohrabi_b@iust.ac.ir

B. Sohrabi
e-mail: sohrabi_b@yahoo.com

Introduction

Carbon nanotubes (CNTs) are structurally unique materials that exhibit excellent mechanical, electrical, thermal, and optical properties [1], and they offer potential promise for a number of novel applications [2, 3]. However, their high aspect ratio and propensity to aggregate into bundles makes disentanglement and dispersion non-trivial processes limiting commercial applicability [4]. In recognition of this problem, development of dispersion technologies based on both chemical and physical approaches has been extensively studied. Chemical functionalization was proposed to be a promising method to improve dispersion of the carbon nanotubes in organic solvents [5–7] as well as in aqueous media [8–12]. However, covalent functionalization disrupts the π-networks of CNTs, which creates possible losses in their mechanical and electrical properties. Thus, attention has turned toward the noncovalent modification to obtain aqueous CNT suspensions. This approach is based on the adsorption of appropriate molecules on the CNT surface, usually surfactants [4, 9, 13], aromatic compounds [14], and polymers [15, 16], which preserves their desired properties.

In the past several years, the noncovalent stabilization by surfactants has been widely used in the preparation of aqueous solutions of individually dispersed CNTs. Among the various surfactants investigated, sodium dodecylbenzenesulfonate (SDBS) [4, 17, 18], sodium dodecyl sulfate (SDS) [4, 17, 18], hexadecyltrimetylammonium bromide (C_{16}TAB) [4, 19], octyl phenol ethoxylate (Triton X-100) [4, 18, 19], and sodium cholate (SC) [17] are the most commonly used. Unfortunately, detailed studies on dispersing nanotubes through surfactant

adsorption sometimes give contradictory results. For example, Islam and coworkers found minimal dispersion in water of single-walled carbon nanotubes (SWNTs) using dodecyltrimethylammonium bromide (C_{12}TAB) [4, 18], while its longer chained relative, hexadecyl based C_{16}TAB imparted substantial aqueous dispersability to both single-walled carbon nanotubes (SWNTs) and multi-walled carbon nanotubes (MWNTs) [4, 19, 20]. These results contrast the reported trend that shorter alkyl chains enhance surfactant effectiveness in dispersing nanotubes due to steric considerations in penetrating and exfoliating nanotube bundles. This illustrates that nanotube diameter plays an important role in surfactant adsorption. Further evidence for this is supported by surfactant adsorption on graphite (negligible curvature nanotubes) in which long chain is preferable [21]. Therefore, one should study effect of the alkyl chain length and effect of the nanotube diameter separately, on the surfactant adsorption process.

The impact of surfactant concentration and the surfactants molecular structure on the number of isolated nanotubes in solution has been systematically investigated in a number of phenomenological studies. However, since the interplay between surfactants and CNTs is complicated and the number of potential control parameters is large, a comprehensive understanding and detailed insight about interaction mechanism between surfactant-CNT and morphology of the surfactant adsorbed on the nanotube surfaces are inevitable for successful dispersion procedure [22]. Currently, three kinds of morphology models have been proposed for surfactant adsorption on the nanotube surfaces. CNTs can be encapsulated within cylindrical micelles [23], or covered with either hemispherical micelles [18, 24] or randomly [25] adsorbed molecules. The binding mechanism between surfactants and nanotube, however, remain a topic of debate. Different arguments over the surfactant-nanotube may result from the situation that these experimental studies originated from various investigated systems, each with different carbon nanotube diameters and different surfactant packing densities. This possibly leads to an incomplete structure picture. On the other hand, in all these studies, surfactant adsorption was not directly measured and the adsorbed structures could not be observed. Besides, it can be difficult to determine the actual surfactant concentration if it is not measured directly because of surfactant adsorption on all kinds of interfaces in the system, including CNTs, container surfaces, and liquid–gas interfaces [22].

Computer simulations do not suffer from the experimental limitation. Using computer simulations we are able to determine directly the actual concentration, the adsorbed amount, and the adsorbed surfactant structures on the nanotube surfaces. Further, it is possible to investigate how the adsorption on CNTs of given diameter may be affected by the molecular architecture of the surfactants. However, the high computational cost of the all-atomistic MD simulations does not allow to simulate large enough systems to determine the adsorption isotherm of surfactant molecules on SWNTs.

The potential of molecular simulations in studying surfactant adsorption on CNTs has been demonstrated by a number of recent studies. Wallace et al. [26] used coarse-grained molecular dynamics to investigate the dependence of adsorbed structures on the bulk concentration and calculated the average orientation of the surfactant molecules with respect to the nanotube axis to characterize the structures formed. Tummala et al. [27] used fully atomistic molecular dynamics (MD) simulations and observed that the morphology of SDS surfactant aggregates strongly depends on the nanotube diameter as well as on the surface coverage. In addition, interactions between two SDS-coated SWNTs have been studied using MD simulations, including elucidating the contributions from electrostatic and vdW interactions to the simulated potential of mean force (PMF) between the two SWNTs [28]. Aqueous dispersions of SWNTs stabilized using the bile salt surfactant SC have been investigated via MD simulations by Lin et al. [29]. Their simulations demonstrated that the cholate ions wrap around the tubes with a small tendency to orient perpendicularly to the tube axis. MD simulations have been used by Tummala et al. [30] to describe the self-assembly of flavin mononucleotide (FMN) adsorbed on SWNTs. They found that the aggregation morphology of aqueous FMN on SWNTs depends on nanotube diameter. Recently, Suttipong and et al. [31] used fully atomistic MD simulations to study the adsorption of sodium dodecylbenzenesulfonate (SDBS) surfactants on SWCNTs from aqueous solution. They showed that the surfactant molecular structure strongly affects the packing of surfactants on the nanotubes, therefore modulating effective nanotube-nanotube interactions.

In this paper, we use a large-scale (up to 34,000 atoms) and all-atomistic MD simulations to study the adsorption and self-assembly of cationic surfactants containing trimethylammonium headgroups (C_{12}TAB and C_{16}TAB) on the SWNT surfaces. The only difference between these two surfactants is number and length of their hydrocarbon tails. In particular, we wished to investigate the behavior of the two cationic surfactants under various surfactant packing densities and SWNT diameters. Furthermore, we study the adsorption and self-assembly of C_{12}TAB and C_{16}TAB in order to clarify the influence of tail length on the adsorption process and structure formed. In our simulations, cationic surfactant monomers and in some cases small micelles will coexist with adsorbed cationic surfactant present in the C_{12}TAB-SWNT or C_{16}TAB-SWNT assembly, which is required for the system to attain thermodynamic equilibrium.

Methods

Computational model

The GROMACS 4.5 software package [32] was employed to perform MD simulations on several systems containing SWNT, cationic surfactants containing trimethylammonium

headgroups (C_{12}TAB or C_{16}TAB), and water. Two SWNTs [(5,7) and (10,14)] of 4.45 nm long and with diameters of 0.82 and 1.64 nm, respectively, were considered. The SWNTs were kept rigid throughout the simulations, with all the carbon atoms in the nanotube treated as uncharged Lennard-Jones (LJ) spheres using the LJ non-bonded interaction parameters which corresponded to the naphthalene OPLS-AA (all-atom optimized molecular potential for liquid simulation) carbon atoms [33]. Water molecules were modeled using the standard SPC/E model [34], with bond lengths constrained using the SETTLE algorithm [35]. Cationic surfactant molecules (C_{12}TAB or C_{16}TAB), which were assumed to completely dissociate into bromide ions and dodecyltrimethylammonium or hexadecyl-trimetylammonium ions were modeled using the OPLS-AA force field and the atomic charges were determined by RESP fit using the RED server [36–39]. The computed atomic charges of dodecyltrimethylammonium and hexadecyl-trimetylammonium ions were summarized in Table S1 and S2 in the Supporting information. Bond lengths in the dodecyltrimethylammonium or hexadecyltrimetylammonium ion were constrained using LINCS algorithm [40]. The long-range electrostatic interactions were handled with the particle mesh Ewald (PME) method [41, 42]. The van der Waals interactions (vdW) were treated with cut off at 1.2 nm. The vdW interactions between different atoms were calculated from the LJ potential using the standard geometric averaging rule which is implemented in the OPLS-AA force field.

The equations of motion were integrated with a time step of 2 fs using the Verlet (Leap-Frog) algorithm [43, 44]. All the simulations were conducted under the NPT ensemble (constant number of atoms, constant pressure of 1.0 bar, and constant temperature of 300 K) in order to best mimic the experimental conditions. Constant temperature and pressure were maintained using the velocity-rescaled Berendsen thermostat [45] and a Parrinello-Rahman barostat [46]. Periodic boundary conditions were applied in all three directions. The trajectories, velocities, and forces corresponding to all the atoms in the system were saved every 1000 steps (2 ps) to satisfy the ergodicity criterion for data analysis [47].

Simulated systems

For all simulated systems, one finite SWNT was maintained at the center of simulation box, with its cylindrical axis oriented along the z-direction. The SWNT was not allowed to move during the simulations using a force constant of 1000 kJ mol^{-1} nm^{-2}. Note that in experiments SWNT solubilization requires sonication, leading to a randomized configuration of surfactant molecules. Therefore we generated our starting configurations by randomly positioning surfactant molecules around a SWNT. Subsequently, the simulation box was filled with water molecules. In order to maintain electroneutrality, an appropriate number of water molecules were replaced by bromide counterions resulting from the added either dodecyl-trimethylammonium or hexadecyltrimetyl-ammonium ions. The simulated systems, including the SWNTs, the total number of surfactant and water molecules, the total number of atoms, and the size of simulation box are presented in Table 1. Because most of the nanotubes were opened after sonication, it is likely that the interior of the nanotube would be accessible to the environment, and potentially filled by the solvent, ions or other molecules. Therefore, the length of the simulation boxes were chosen to be longer than the nanotubes length to allow the water molecules or bromide ions to fill the nanotubes. Before initiating the MD simulations, an energy minimization was performed using the steepest decent method to relax the systems. Each system was equilibrated for 12 ns, and only the last 5 ns of simulation were used for data analysis. Although this time scale is too short to entirely understand the true dynamic properties of surfactant adsorption onto SWNT, the simulations can provide dynamical information about the surfactant structures which is representative of the processes occurring in these systems. To show the simulated systems have reached the stable minimum, we plotted the variation of solvent accessible surface (SAS) areas of the dodecyltrimethylammonium and hexadecyl-trimetylammonium ions as a function of simulation time (see Fig. S1 in the Supporting information). SAS area was traced out by a probe sphere of radius 0.14 nm which was rolled around the dodecyltrimethylammonium or hexadecyl-trimetylammonium ions to identify their solvent accessible surface areas.

Results and discussion

C_{12}TAB adsorption and surface self-assembly on a SWNT

To study the influence of the surfactant concentration on the adsorption and surface morphology of aggregates formed on a nanotube surface, we randomly positioned an increasing number of C_{12}TAB molecules (12, 19, and 26) around a SWNT (5,7). Different numbers of C_{12}TAB molecules

Table 1 Simulation details for the systems studied in this work

System	SWNT	N_{C12TAB}	N_{C16TAB}	N_{water}	$N_{total\ atoms}$	Box size (nm^3)
1	(5,7)	12		11002	34054	7×7×7
2	(5,7)	19		10893	34084	7×7×7
3	(5,7)	26		10749	34009	7×7×7
4	(5,7)		12	10967	34093	7×7×7
5	(5,7)		26	10644	34006	7×7×7
6	(10,14)	24		10581	33839	7×7×7
7	(10,14)		24	10473	33803	7×7×7

added correspond to different surface packing density, with 12, 19, and 26 added C_{12}TAB molecules corresponding to the original surface coverage of 1.05 (low surface coverage), 1.66 (moderate surface coverage), and 2.27 (high surface coverage) molecule/nm^2, respectively. The original surface coverage is computed based on the SWNT diameter and length as well as the number of surfactant molecules present at the simulation box. All of surfactant packing densities are comparable to those known for SDS and SDBS [27, 31]. Representative simulation snapshots of a SWNT (5,7) covered by C_{12}TAB molecules are shown in Fig. 1. As can be observed in Fig. 1, there is a clear correlation between the C_{12}TAB surface coverage and aggregates formed on the nanotube surfaces. At low surface coverage, there is sufficient space on the nanotube surface to fit the C_{12}TAB molecules and therefore C_{12}TAB molecules prefer to lie parallel to the nanotube axis, as can be seen in panel a Fig. 1. This conformation of C_{12}TAB molecules exposes large areas of the hydrophobic C_{12}TAB tails to the aqueous environment and positions the hydrophilic C_{12}TAB heads close to the nanotube surface however, the number of surfactant tail-carbon atoms contacts increases when the C_{12}TAB surfactants lie flat on the nanotube surface. Consequently, the hydrophobic interactions between surface of a SWNT and C_{12}TAB tails increase and make the C_{12}TAB-SWNT assembly stable. An important feature that can be seen in panel a Fig. 1 is that the adsorbed C_{12}TAB molecules prefer to self-assemble next to each other. Presumably this occurs so that C_{12}TAB molecules are able to maximize their tail-tail interactions. The binding or condensation of negatively charged bromide ions contribute also in shielding some portions of the electrostatic repulsion between C_{12}TAB heads and keep C_{12}TAB molecules next to each other. As the C_{12}TAB surface coverage increases the available nanotube surface area per C_{12}TAB molecule reduces thereby, C_{12}TAB molecules adsorb at shorter distance on the nanotube surface. Consequently, both the electrical charge repulsions between C_{12}TAB heads and the repulsions between tail-head neighboring C_{12}TAB molecules become stronger. At this condition, C_{12}TAB molecules either bend and wrap around the nanotube surface or extend their heads toward the aqueous phase, as can be seen in panel b in Fig. 1. For higher surface coverage, there is little tube surface area available per C_{12}TAB molecule, the repulsions just described become even stronger and as a result the orientation of C_{12}TAB molecules on nanotube surface is completely changed in comparison to low surface coverage (see panel a and c Fig. 1). As can been observed in panel c Fig. 1, most C_{12}TAB tails wrap around the nanotube surface and the headgroups protrude toward the aqueous phase. In

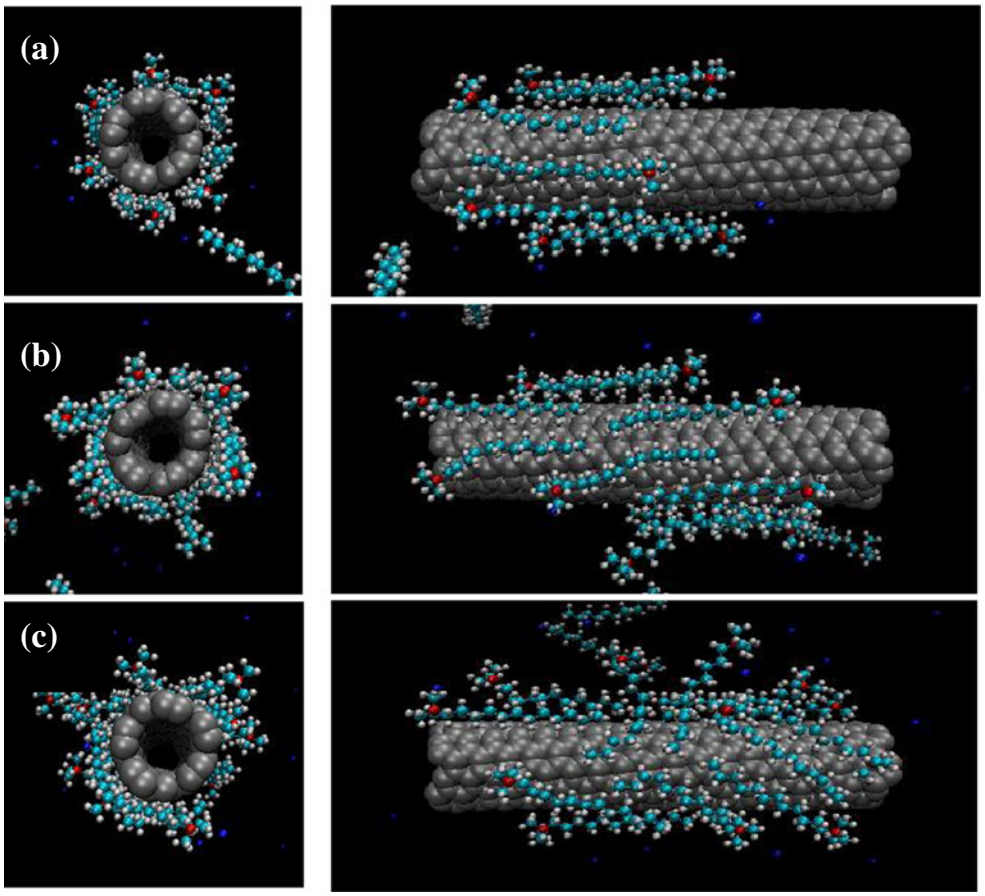

Fig. 1 Representative simulation snapshots of a (5,7) SWNT in aqueous C_{12}TAB solutions at three different surface packing densities **a** 1.05 molecule/nm^2, **b** 1.66 molecule/nm^2, and **c** 2.27 molecule/nm^2. The three plots on the right are side views, and the three plots on the left are corresponding front views. Water molecules are not shown for clarity. Color code: red, nitrogen; blue, bromide counterion; cyan, carbon; white, hydrogen; silver, carbon atoms in the SWNT. Images are rendered by using VMD visualization suite [48]. All snapshots are at the 12 ns in the MD simulations

addition, few C_{12}TAB adsorbed stand up on the nanotube surface such that fewer C_{12}TAB tail particles are in direct contact with the nanotube surface. Presumably this occurs so that more C_{12}TAB molecules are able to incorporate into C_{12}TAB-SWNT assembly. Moreover, this orientation of C_{12}TAB molecules makes the hydrophobic surface of the SWNT and C_{12}TAB tails shielded from the aqueous environment.

To investigate the C_{12}TAB adsorption mechanism on the SWNT and to elucidate the orientation of aggregates formed under different original surface coverages, we calculate the orientation of C_{12}TAB molecules with respect to the SWNT axis. The angle between C_{12}TAB molecules and the SWNT axis is defined by

$$\theta = \arccos\left(\frac{\vartheta_{SWNT}\cdot\vartheta_{SUR}}{|\vartheta_{SWNT}||\vartheta_{SUR}|}\right) \quad (1)$$

where ϑ_{SUR} is the vector from the carbon atom at the end of the dodecyl chain of C_{12}TAB surfactant to the nitrogen atom in the trimethylammonium group (defined in Fig. 2) and ϑ_{SWNT} is the SWNT axis vector. The θ angle formed between the surfactant molecule and the nanotube axis can be either wrapping angle or contact angle, as illustrated in Fig. 2. If a surfactant molecule is wrapped around the SWNT, the θ angle can be described as a wrapping angle, or alternatively, if a surfactant molecule is rotated away from the nanotube surface, in which case, the θ angle can be considered as a contact angle. Note that when the angle between the C_{12}TAB surfactants and the SWNT axis is 0° or 180°, the correspondent vector is parallel to the nanotube axis. When this angle is 90°, the vector is perpendicular to the nanotube axis.

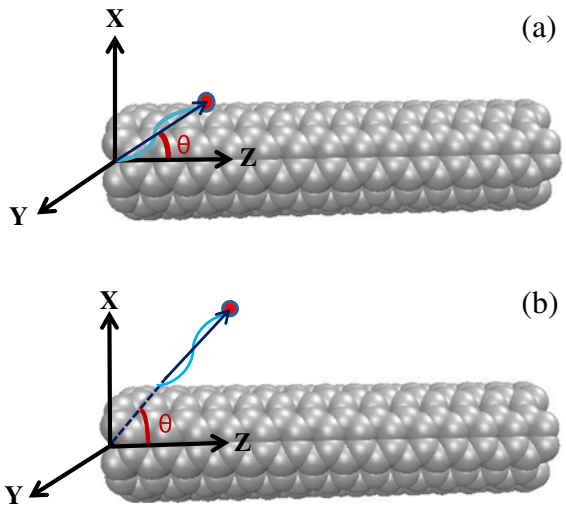

Fig. 2 **a** Illustration of a surfactant molecule wrapping around a SWNT and formation of a wrapping angle θ with respect to the SWNT axis. **b** Illustration of a surfactant molecule rotated away from the tube surface and formation of a contact angle θ between the surfactant and the nanotube

The orientation distribution for C_{12}TAB surfactant molecules at three different surface packing densities are shown in Fig. 3. At low surface coverage, the largest peaks are close to 0° and 180°, indicating that C_{12}TAB molecules tend to orient almost parallel to the SWNT axis. This result is consistent with observations in recent MD simulations of SDS and SC self-assembly on the nanotube surface [27, 29]. However, unlike the SDS and C_{12}TAB surfactants, SC surfactant also have a tendency to orient almost perpendicular to the nanotube axis at low surface coverage to accommodate their slightly bent planar chemical structures with respect to the curved nanotube surface. The same orientation of SDS and C_{12}TAB molecules to the SWNT axis suggests that the surfactant headgroup size and the counterion radius do not play a major role at low surface coverage in morphology of aggregates formed on the SWNT surfaces (both SDS and C_{12}TAB have the same tailgroup). Upon increasing the surface coverage, the probability of parallel orientation of C_{12}TAB decline. Instead, C_{12}TAB molecules prefer to wrap around the SWNT and form various wrapping angle with respect to the nanotube axis. Note that for the case of high surface coverage, C_{12}TAB molecules have a small tendency to orient almost perpendicular with respect to the SWNT axis, in which case, they form the contact angle with the nanotube surface. These results further confirm that arrangement of the C_{12}TAB adsorbed depends on the surface coverage. Our simulations demonstrate that at low surface coverage the entire C_{12}TAB tails and heads are in direct contact with the nanotube surface and they form the angles close to the 0° or 180° with respect to the SWNT axis which is more consistent with the random adsorption model. However, it seems that upon increasing the surface coverage, the C_{12}TAB adsorption mechanism gradually changes such that at high surface coverage C_{12}TAB molecules either wrap around the nanotube or stand up in a "tails on" configuration [23]. For this reason, our results suggest that a cylindrical model may be preferred for surfactant high packing density, although additional simulations at higher surface coverage are necessary to further corroborate this suggestion.

To clarify the C_{12}TAB adsorption mechanism on nanotube, we plot the radial distribution function (RDF) of tail and head segments with respect to the axis of the tube at three different surface coverages. As can be observed in Fig. 4, a common feature shared by three tail segment RDF curves is that all display one strong peak at ~ 0.8 nm, confirming the C_{12}TAB tails adsorb on the nanotube surfaces and form an adsorption monolayer as well. Similar results have been reported for the case of SDS and SDBS adsorption onto SWNT at low surface density [27, 31]. However, our results demonstrate the formation of monolayer structure even at high surface density, whereas a second shell of tail segments has been formed for SDS adsorption onto SWNT at high surface density [27]. The tail segment RDF profiles in Fig. 4 further indicate that the thickness of an adsorption monolayer increases from ~ 0.3 to

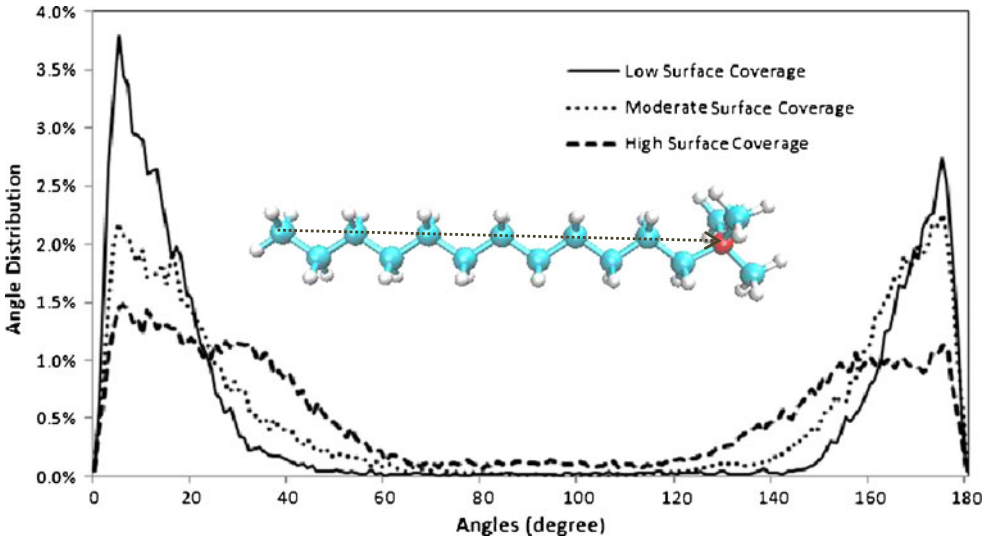

Fig. 3 Simulated distribution profiles of the angle formed between the vector of the dodecyltrimethylammonium ions and the SWNT axis. Results are obtained for the systems shown in Fig. 1. In the dodecyltrimethylammonium structure shown, the dotted line connecting the nitrogen atom in the trimethylammonium group with the carbon atom at the end of the dodecyl chain defines the axis of the dodecyltrimethylammonium ion

0.5 nm and the peak intensity decreases upon increasing the surface coverage. This suggests that C_{12}TAB tails are rotated away from the SWNT surface such that fewer C_{12}TAB tail particles are located adjacent to the nanotube surface. This orientation of C_{12}TAB tails causes a smaller amount of water molecules can be found near the nanotube surface (see Fig. S2 in the supporting information for more details). The head segment RDF curves for all surface densities demonstrate one obvious peak at ~ 0.9 nm in which overlap with the tail segment curves. In the case of low surface coverage, the profile clearly shows that most C_{12}TAB heads are located near the nanotube surfaces and almost the same position of C_{12}TAB tails and only a small fraction of the C_{12}TAB heads are positioned further and extended to the aqueous phase, as can be noticed from the shoulder found at ~ 1.2 nm in panel a Fig. 4. This result confirms that the random adsorption can be appropriately used to model C_{12}TAB adsorption at low surface density. As the surface density increases, the shoulder becomes stronger and broader, indicating that more C_{12}TAB heads are located further from the nanotube surface and pointed outward to the water. This observation along with the thickness increase of the adsorption monolayer at high surface density may propose that there is a transition in interaction mechanism upon increasing the surface coverage from random adsorption to cylindrical adsorption. Our MD simulation results at low and high surface coverage have been experimentally reported for the self-assembly structure of the CTAB and SDS surfactant adsorbed on the SWNT [23, 49].

As mentioned earlier, counterion-condensation phenomena contribute in shielding some portions of the electrostatic repulsion between C_{12}TAB heads. This feature can be seen in Fig. 5, where we plot the RDF profile of bromide ions respect to the axis of the tube at three different surface densities. As can be observed in Fig. 5, bromide ions accumulate near the C_{12}TAB heads and neutralize some parts of head charges. As the distance r increases the counterion RDF profiles decay slowly. These results confirm that SWNT-C_{12}TAB complexes can be thought of as polyanions, in which counterion condensation does not manage to neutralize the entire complex charge, as has been reported by Manning [50–52]. Similar simulation results have been observed in the case of SDS and SC adsorption onto SWNTs [27, 29].

Tail length effect: C_{16}TAB adsorption on a SWNT

To examine the influence of the tail length on nanotube adsorption we perform self-assembly simulations of C_{16}TAB surfactant molecules around the SWNT (5,7) at conditions comparable to those considered above. For this purpose, we randomly position either 12, or 26 C_{16}TAB molecules around the nanotube in which 12, and 26 added C_{16}TAB molecules corresponding to the original surface coverage of 1.05 (low surface coverage), and 2.27 (high surface coverage) molecule/nm^2, respectively. Representative simulation snapshots of C_{16}TAB adsorbed on a (5,7) SWNT at low and high surface coverages are shown in Fig. 6. Visual inspection of simulation snapshots at low surface coverage indicate that C_{16}TAB molecules align parallel respect to the nanotube axis, consistent with the C_{12}TAB study. Undoubtedly this orientation of C_{16}TAB molecules must be attributed to the hydrophobic interactions between surfactant tail-carbon SWNT. Compared to the C_{12}TAB surfactant, the number and length of hydrocarbon tails in C_{16}TAB have been increased. Thus, there is a stronger repulsion between tail-head neighboring C_{16}TAB molecules with antiparallel orientation. This repulsion along with an electrostatic repulsion between heads make the C_{16}TAB heads protrude pronouncedly toward the aqueous phase, as can be seen in panel a Fig. 6 (see also panel a Fig. 1). As mentioned earlier for the C_{12}TAB study, upon increasing the original surface coverage, surfactant molecule

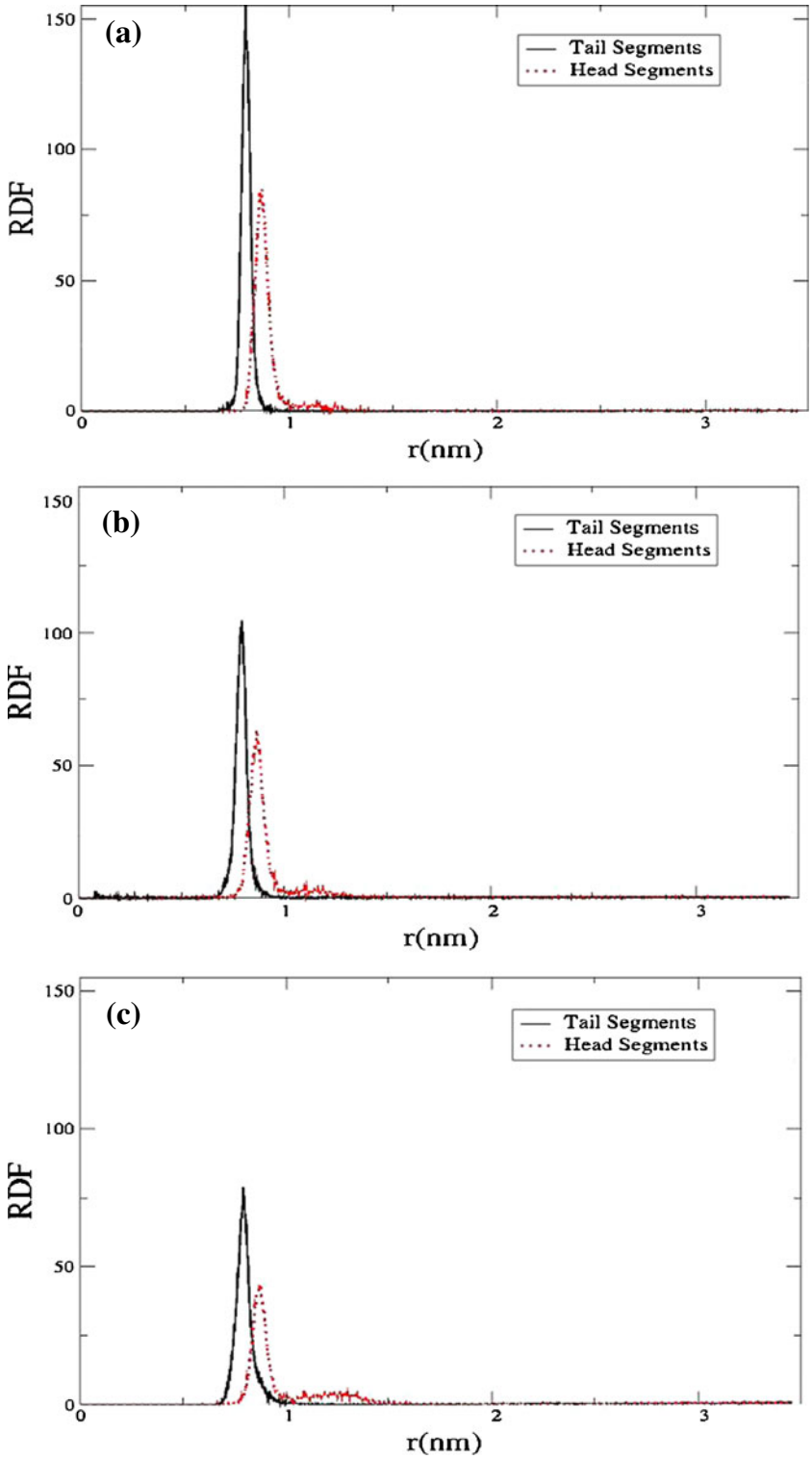

Fig. 4 Simulated radial distribution functions (RDFs) of C_{12}TAB tail and head segments around the CNT as a function of the distance from the axis of the tube at three different surface packing densities **a** 1.05 molecule/nm^2, **b** 1.66 molecule/nm^2, and **c** 2.27 molecule/nm^2

adsorb at shorter distance on the nanotube surface so both the head-head and tail-head repulsions increase and make the C_{12}TAB molecule either wrap around the tube or C_{12}TAB heads protrude toward the aqueous phase. For the C_{16}TAB surfactant at high surface coverage (2.3 molecule/nm^2), the nanotube surface area available per C_{16}TAB tail particle has been reduced in comparison to the C_{12}TAB study. Note that the tube surface area available per C_{16}TAB molecule is the same as the C_{12}TAB molecule. However, C_{16}TAB has a longer hydrocarbon tail which leads to the reduction of the tube surface area available per C_{16}TAB tail particle. Therefore, packing of the C_{16}TAB molecule on the SWNT surface is

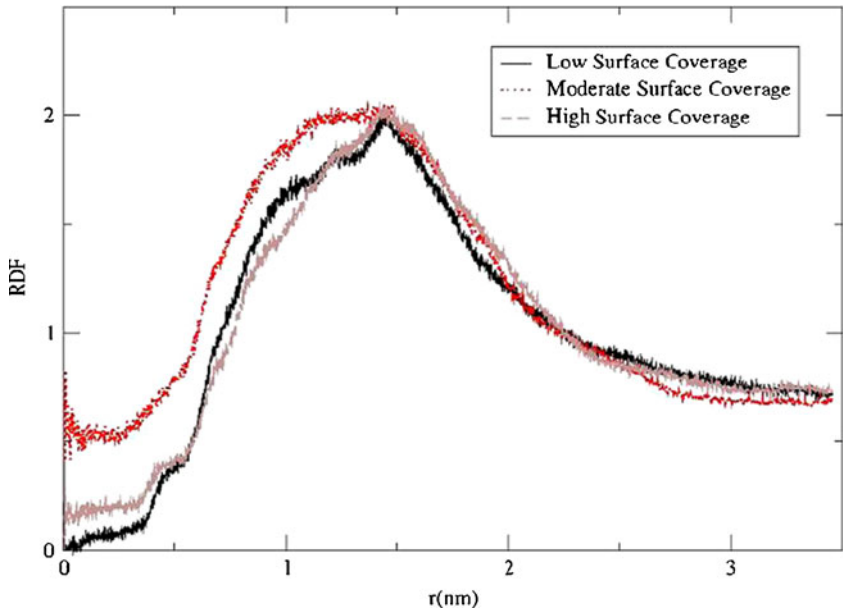

Fig. 5 Simulated radial distribution functions (RDFs) of bromide counterions around the CNT as a function of the distance from the axis of the tube at three different surface packing densities which correspond to the systems shown in Fig. 1

more difficult than C_{12}TAB molecule. Consequently, the difficulty of packing of longer molecule along with the head-head and tail-head repulsions make the C_{16}TAB heads protrude more pronouncedly toward the aqueous phase and fewer tail particles (even compared to C_{12}TAB study) being in contact with the tube as well, as can be observed in panel b Fig. 6. Presumably this transition in adsorption mechanism occurs so that more C_{16}TAB molecules are able to incorporate into the C_{16}TAB-SWNT assembly, thereby minimizing exposure of the hydrophobic SWNT and the C_{16}TAB tails to the aqueous environment. In addition, we point out that C_{16}TAB molecules do not wrap around the SWNT at high surface coverage, inconsistent with the C_{12}TAB study. This may be attributed to the C_{16}TAB longer tail which increases the energetic cost for wrapping the molecule around the nanotube circumference.

In order to elucidate the C_{16}TAB adsorption mechanism under low and high surface coverages and to reach a better understanding of the influence of the tail length on the SWNT adsorption, we calculate the angle between the vector identified by the axis of the C_{16}TAB molecule (defined in Fig. 7) and the axis of the nanotube according to Eq. 1. The orientation distribution for C_{16}TAB surfactants at two different surface coverages are shown in Fig. 7. As shown in Fig. 7,

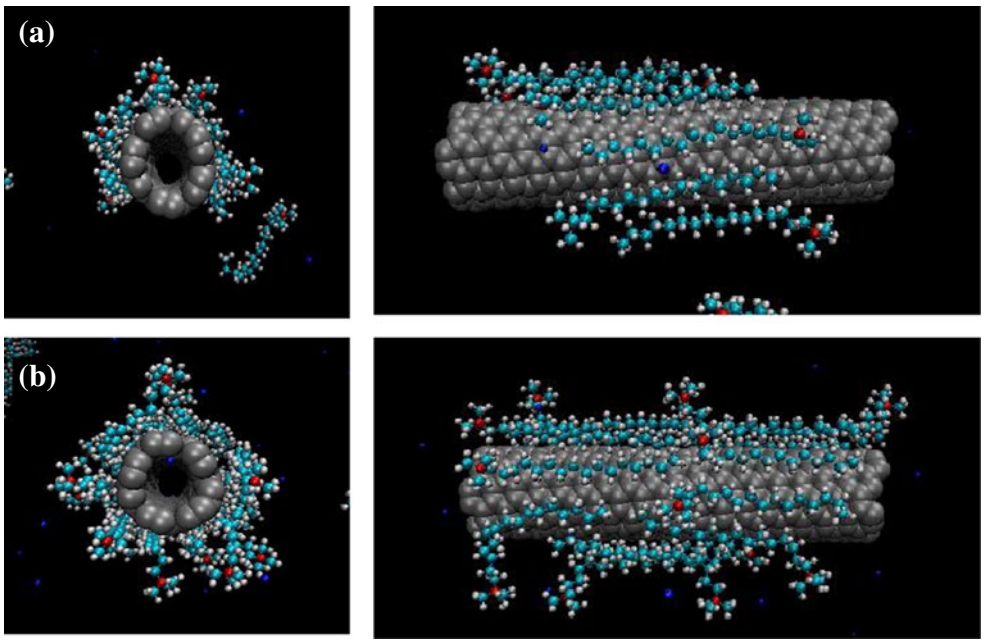

Fig. 6 Representative simulation snapshots of a (5,7) SWNT in aqueous C_{16}TAB solutions at two different surface packing densities **a** 1.05 molecule/nm^{2}and **b** 2.27 molecule/nm^2. The two plots on the right are side views, and the two plots on the left are corresponding front views. Water molecules are not shown for clarity. The color code is the same as that used in Fig. 1. Images are rendered by using VMD visualization suite. All snapshots are at the 12 ns in the MD simulations

there is a clear correlation between the surface coverage and the C_{16}TAB orientation. At low surface coverage, there are two obvious peaks~10° and 170°, indicating that C_{16}TAB molecules tend to orient nearly parallel with respect to the nanotube axis. Compared to the C_{12}TAB and SDS molecules, the angles formed between C_{16}TAB axis and the SWNT axis are larger which can be attributed to the fact that C_{16}TAB heads protrude pronouncedly toward the water. For high surface coverage, Fig. 7 displays four broad peaks at around 10°,60°,120°, and 170° in which the positions of two peaks are the same as those observed at low surface coverage. This indicates that at high surface coverage, some C_{16}TAB orient nearly parallel to the SWNT axis and only their heads point toward the aqueous phase. However, two peaks at around 60° and 120° demonstrate that upon increasing the surface coverage, the orientation of some C_{16}TAB molecules change such that not only their heads protrude toward the water but also their tail particles stand up and rotate away from the SWNT surface. Figure 7 also shows that upon increasing the surface coverage, the C_{16}TAB tendency to form various contact angles with respect to the nanotube axis increases. Compared to the C_{12}TAB study, the C_{16}TAB tendency for being perpendicular with respect to the SWNT axis has been increased. Therefore, our results at high surface coverage seem to be in line with the hypothesis that surfactant form cylindrical micelles on the SWNT surface. However, for low surface coverage a random adsorption model is thought to be more consistent with our simulations. The C_{16}TAB adsorption mechanisms for both low and high surface coverages are in agreement with our C_{12}TAB study and the experimental results of CTAB adsorption on nanotube [49].

In order to attempt to clarify the role of surfactant tail length on the surface isolation of carbon nanotube from the environment, we compare the radial distribution function (RDF) of water molecules with respect to the axis of the tube for the systems contain either C_{12}TAB or C_{16}TAB surfactants at different original surface coverages. Figure 8 shows that at low original surface coverage, the position and intensity of peaks for both C_{12}TAB and C_{16}TAB surfactants are the same, indicating that there is no difference between the amounts of water molecules near the nanotube surface for both systems. However, as will be described in more detail in the next section, the amount of C_{16}TAB adsorbed onto (5,7) SWNT at low surface coverage is smaller than that for C_{12}TAB (see Table 2). This fact indicates that C_{16}TAB surfactant are more effective at shielding the nanotube surface from being in contact with water molecules. Note that the high intensity peaks around 0.1 nm are due to the water molecules in the interior of the SWNTs. For high surface coverage, the peak intensity around 0.75 nm as well as the shoulder intensity found around 1 nm decreases for the system that contains C_{16}TAB molecules, implying that C_{16}TAB can effectively decrease the interaction between water molecules and the SWNT surface. Therefore, our simulations prove that the C_{16}TAB surfactant can more strongly isolate the SWNT surface from the environment (in this case water molecules) even when the C_{12}TAB coverage is denser on the SWNT surface than in C_{16}TAB. One of possible reasons for the better isolation of nanotube surface in C_{16}TAB can be attributed to the morphology of aggregates formed at these systems. It is worth pointing out that at low surface coverage and particularly at high surface coverage C_{16}TAB heads protrude pronouncedly toward the aqueous environment in comparison to the C_{12}TAB study. Since previous calculations for the potential of mean force between nanotubes in the presence of aqueous surfactants have demonstrated that the surfactant heads ability to orient perpendicularly to the nanotube axis promote long-ranged repulsive forces between the nanotubes and lead to the effective stabilization of aqueous dispersions [30], therefore it is reasonable to conclude that C_{16}TAB ability to stabilize SWNTs in aqueous suspensions is better than C_{12}TAB.

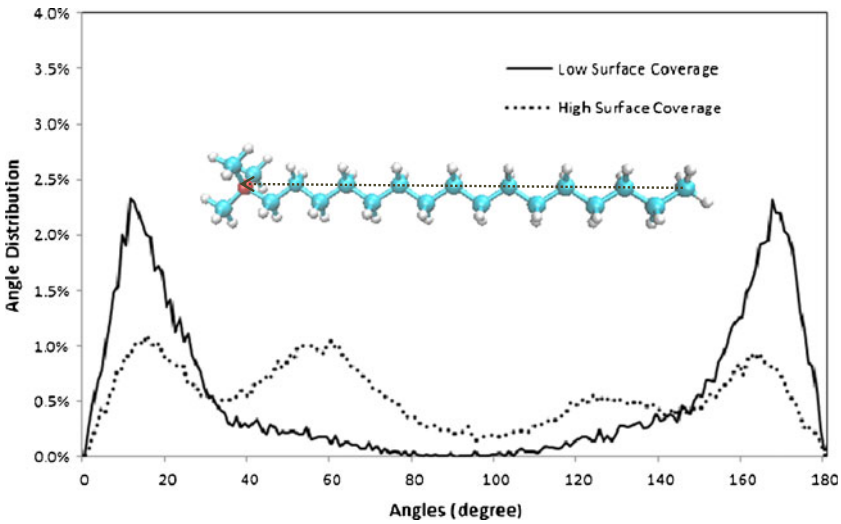

Fig. 7 Simulated distribution profiles of the angle formed between the vector of the hexadecyltrimetylammonium ions and the SWNT axis. Results are obtained for the systems shown in Fig. 6. In the hexadecyltrimetylammonium structure shown, the dotted line connecting the nitrogen atom in the trimethylammonium group with the carbon atom at the end of the hexadecyl chain defines the axis of the hexadecyltrimetylammonium ion

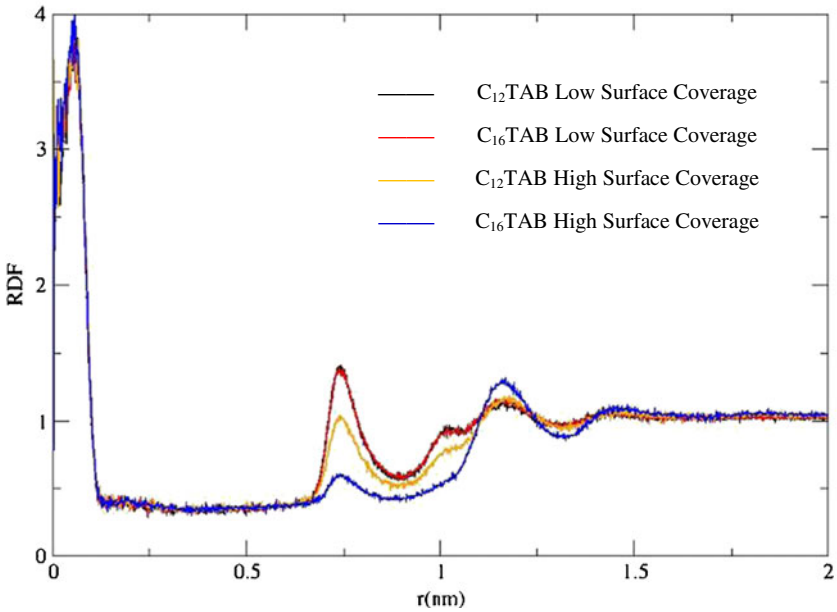

Fig. 8 Simulated radial distribution functions (RDFs) of water molecules around the CNT as a function of the distance from the axis of the nanotube (5,7) for the systems contain either C_{12}TAB or C_{16}TAB surfactants at low surface coverage (1.05 molecule/nm^2) and high surface coverage (2.27 molecule/nm^2)

To deepen our understanding of interaction mechanism between C_{16}TAB-SWNT and morphology of the C_{16}TAB adsorbed on the nanotube surfaces and to compare the C_{16}TAB and C_{12}TAB adsorption, we plot the radial distribution function (RDF) of C_{16}TAB tail and head segments with respect to the axis of the tube at two different original surface coverages. As shown in Fig. 9, both tail segment RDF curves at low and high surface coverages display one strong peak~0.8 nm, indicating that C_{16}TAB tails have been adsorbed as a monolayer on the nanotube surface, consistent with the C_{12}TAB study. For low surface coverage, panel a Fig. 9 illustrates that a majority of C_{16}TAB heads are positioned adjacent to the nanotube surface and C_{16}TAB tails, as can be identified from the obvious peak at around 0.9 nm which overlaps with the tail segments profile. A small portion of C_{16}TAB heads tend to be exposed to water, as can be noticed from the shoulder found at around 1.1 nm in panel a Fig. 9. However, at high surface coverage, we observe two noticeable peaks found at~0.9 and 1.2 nm, in which the first one indicates that some of the C_{16}TAB heads are located near the nanotube surface and the C_{16}TAB tails as well and the latter confirms that some of the C_{16}TAB heads prefer to position further from the nanotube surface and extend to water (see panel b Fig. 9). Compared to the C_{12}TAB adsorption, a greater number of C_{16}TAB heads have been extended to the water. Hence, our results demonstrate that there is a transition in adsorption mechanism upon increasing the surface coverage. At low surface coverage, C_{16}TAB heads and tails are located at the same position, suggesting the random structure, while for high surface coverage a cylindrical structure may be preferable. It is worth pointing out that the structure of C_{12}TAB and C_{16}TAB aggregates formed at high surface coverage on the SWNT considered here are different compared to those obtained on flat graphite surfaces. As previously shown in the literature, molecular dynamics simulations [53], in agreement with experimental atomic force microscopy (AFM) measurements

Table 2 Population analysis results for C_{12}TAB and C_{16}TAB on SWNTs

system	Original surface coverage (S_{or}) molecule/nm^2	Average number of C_{12}TAB adsorbed	Average number of C_{16}TAB adsorbed	Average number of non-adsorbed surfactant	Effective surface coverage (S_{ef}) molecule/nm^2	Excess surface coverage (S_{ex}=S_{or}- S_{ef}) molecule/nm^2
1	1.05	9.91		2.09	0.86	0.19
2	1.66	12.72		6.28	1.11	0.55
3	2.27	15.79		10.21	1.38	0.89
4	1.05		8.00	4.00	0.70	0.35
5	2.27		17.98	8.02	1.57	0.70
6	1.05	20.27		3.73	0.88	0.17
7	1.05		22.00	2.00	0.96	0.09

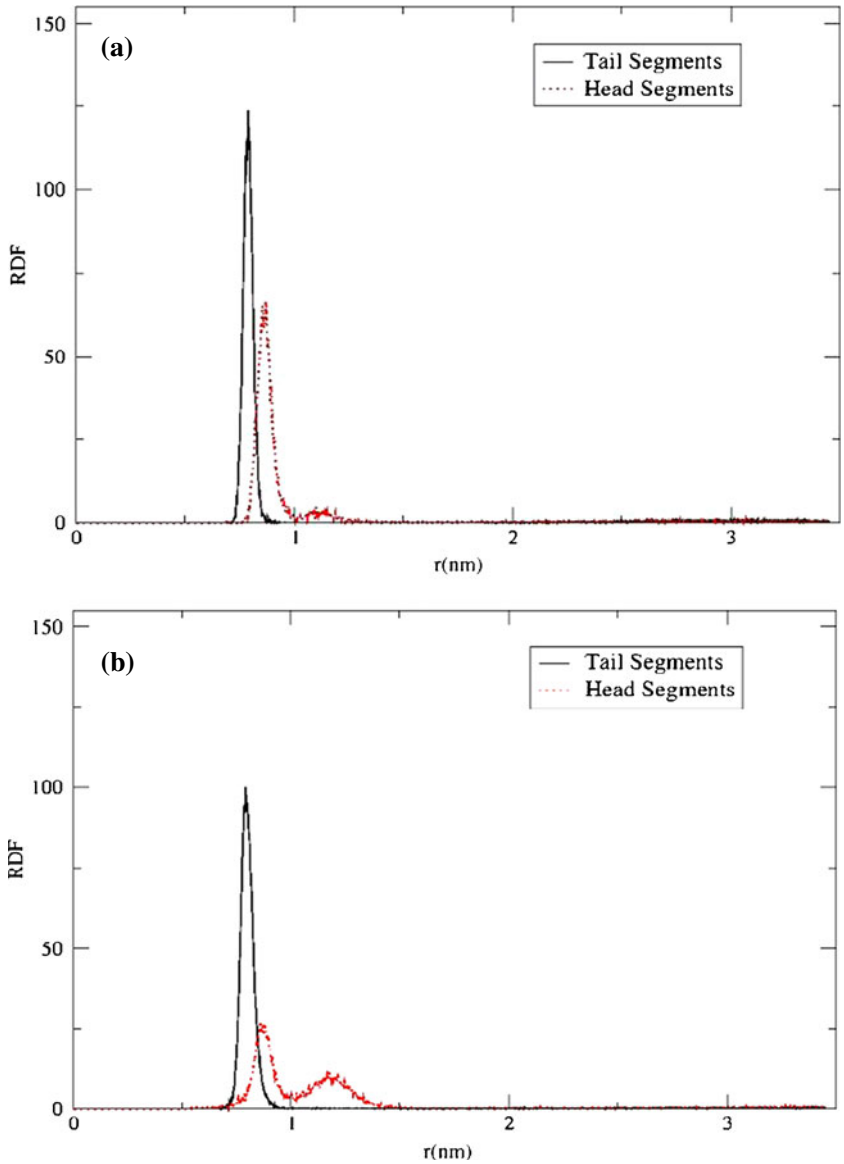

Fig. 9 Simulated radial distribution functions (RDFs) of C_{16}TAB tail and head segments around the CNT as a function of the distance from the axis of the tube at two different surface packing densities **a** 1.05 molecule/nm^2 and **b** 2.27 molecule/nm^2

[54, 55] of cationic surfactants containing trimethylammonium headgroups (C_{16}TAB and C_{14}TAB), adsorbed on graphite at high surfactant density yield hemicylindrical type of aggregates. One of the possible causes of the difference observed in surfactant aggregates morphology can be attributed to the high curvature nanotube surface.

SWNT diameter effect

Lastly, we investigate whether or not the SWNT diameter has an effect on the C12TAB and C16TAB adsorption and the morphology of aggregates formed under low surface coverage. We study the morphology of the surfactant aggregates at low surface coverage because such aggregates provide a template to those formed at higher surface coverage. To perform simulations, we randomly position either 24 C_{12}TAB or 24 C_{16}TAB molecules around a SWNT (10,14), corresponding to the original surface coverage of 1.05 (low surface coverage) molecule/nm^2. Figure 10 shows the views of the representative simulation snapshots of the C_{12}TAB and C_{16}TAB adsorbed on a (10,14) SWNT at low surface coverage. Visual inspection of simulation snapshots for C_{12}TAB surfactant indicate that some of the C_{12}TAB tails align with the nanotube axis, whereas some of the C_{12}TAB tails prefer to wrap around the nanotube, as can be seen in panel a Fig. 10. It is clear that the hydrophobic interaction between the nanotube surface and surfactant tails is responsible for these kinds of orientations. However, we did not observe C_{12}TAB tails wrapped around the narrow (5,7) SWNT at low surface coverage. Presumably, this is because the energetic cost for C_{12}TAB molecules to wrap around a narrow tube is higher. Hence, upon increasing the SWNT diameter, it becomes easier for C_{12}TAB molecule to wrap around the

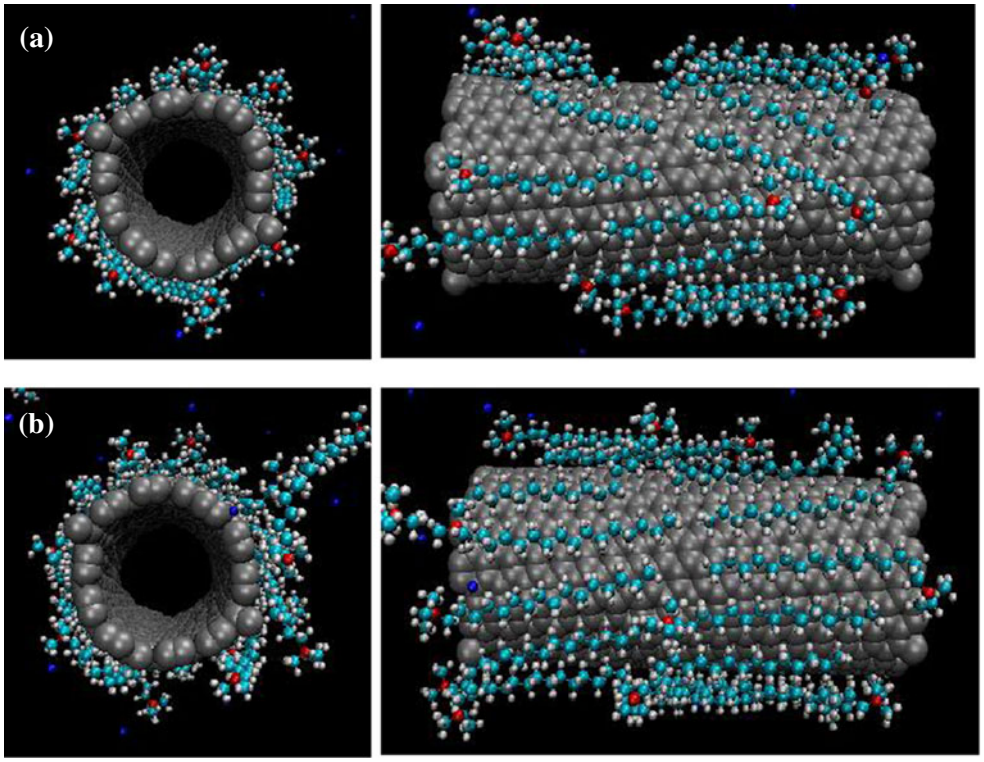

Fig. 10 Representative simulation snapshots of a (10,14) SWNT in aqueous solutions of **a** C_{12}TAB and **b** C_{16}TAB at surface packing density of 1.05 molecule/nm^2. The two plots on the right are side views, and the two plots on the left are corresponding front views. Water molecules are not shown for clarity. The color code is the same as that used in Fig. 1. Images are rendered by using VMD visualization suite. All snapshots are at the 12 ns in the MD simulations

nanotube. Similar to the C_{12}TAB adsorption on a (5,7) SWNT, most of C_{12}TAB heads are located near the (10,14) SWNT surface and C_{12}TAB tails. Obviously, the binding of negatively charged bromide ions contribute in shielding some portions of the electrostatic repulsion between C_{12}TAB heads and give rise to the C_{12}TAB adsorb next to each other.

One clear difference between the C_{12}TAB and C_{16}TAB adsorption on a (10,14) SWNT is that a large number of C_{16}TAB tails prefer to align with the nanotube axis and do not wrap around the SWNT surface (see panel b Fig. 10). As pointed out earlier, this is probably because C_{16}TAB has a longer tail which increases the energetic cost for wrapping the molecule around the nanotube circumference. Another difference between these two systems is that C_{16}TAB heads protrude pronouncedly toward the aqueous phase.

In order to quantify the effective surface coverage of both C_{12}TAB and C_{16}TAB for all our systems studied as well as to clarify the role of tail length on the adsorption process, we compute the time-averaged number of either C_{12}TAB or C_{16}TAB adsorbed on the SWNT. A surfactant molecule is assumed to be adsorbed on the nanotube surface if the distance between the surfactant center of mass and center of mass of the SWNT (5,7) and SWNT (10,14) is up to 1.9 and 2.3 nm, respectively, and the surfactant molecules that are beyond the cutoff distance are considered as dispersed in the aqueous phase which can be found as monomers and, in some cases (at high surface coverage systems), as small aggregates. The average number of non-adsorbed surfactants is calculated as the difference between the total number of surfactant molecules present in the simulation box and the average number of surfactant molecules adsorbed on the nanotube surface. Subsequently, the surfactant effective surface coverage is computed based on the SWNT diameter and length as well as the number of surfactant molecules adsorbed on the SWNT surface. In addition, estimating the excess surface coverage is quite straightforward. Specifically, the excess surface coverage is equal to the difference between the original surface coverage and the effective surface coverage. Detailed results of population analysis for both C_{12}TAB and C_{16}TAB molecules at low and high surface coverages have been reported in Table 2.

As can be seen in Table 2, for C_{12}TAB adsorption on a (5,7) SWNT at low, moderate, and high surface coverages, corresponding to the systems 1 to 3, both the number of C_{12}TAB surfactant adsorbed on the nanotube surface and the number of non-adsorbed C_{12}TAB molecules in the aqueous phase away from the nanotube increase upon increasing the original surface coverage. Consequently, the effective C_{12}TAB surface coverage increases from 0.86 to 1.38 molecule/nm^2 and the excess C_{12}TAB surface coverage increases from 0.19 to 0.89 molecule/nm^2 as well. Note that the increase of the excess surface coverage upon increasing the original surface coverage is sharper than the increase of the effective surface coverage. This fact indicates that upon increasing the original surface coverage, the number of non-adsorbed surfactant molecules would be larger than the number of the C_{12}TAB adsorbed on the nanotube surface. For the C_{12}TAB adsorption

at low surface coverage on a (10,14) SWNT, corresponding to system 6, the values of both the effective and excess C_{12}TAB surface coverages are almost the same as those obtained for the case of low C_{12}TAB surface coverage on a (5,7) SWNT (system1). Therefore, our results demonstrate that effect of the SWNT diameter on the effective surface coverage of the C_{12}TAB molecule is weak. Similar results have been reported in the case of SDBS adsorption onto SWNT [31].

For the C_{16}TAB adsorption on a (5,7) SWNT, corresponding to the systems 4 and 5, both the effective C_{16}TAB surface coverage and the excess C_{16}TAB surface coverage have been increased, consistent with the C_{12}TAB surfactant. However, the increase of the excess surface coverage upon increasing the original surface coverage is weaker than the increase of the effective surface coverage. It means that with increasing the original surface coverage, the number of C_{16}TAB adsorbed on the nanotube surface increases more than the number of the non-adsorbed surfactant molecules. This result contrasts with the C_{12}TAB case, where the number of adsorbed C_{12}TAB molecules is smaller. This different behavior may be due to the fact that the C_{16}TAB has a longer chain which increases the hydrophobic interactions between surfactant tail particles and makes favorable the adsorption of C_{16}TAB molecules by increasing the original surface coverage. Thus, our results suggest that the effective surface coverage is influenced not only by the hydrophobic interactions between surfactant tails and the SWNT but also the hydrophobic interactions between surfactant tails. Note that upon increasing the number of surfactant molecules present in the simulation box, the effect of the surfactant tails interactions on the effective surface coverage become stronger. For this reason the value of effective C_{16}TAB surface coverage obtained for the adsorption of C_{16}TAB on a (10,14) SWNT (system 7) has been substantially increased in comparison to the C_{16}TAB adsorption on a (5,7) SWNT.

For C_{16}TAB adsorption on a (5,7) SWNT at low surface coverage (system 4), the value of the effective surface coverage is smaller than that obtained for the case of C_{12}TAB. This is because only 12 surfactants are present at the simulation box at these systems. Presumably, the influence of the hydrophobic interactions between surfactant tails on the effective surface coverage is weak. Hence, at these systems the hydrophobic interactions between surfactant tails and the SWNT surface is dominant and since for the C_{16}TAB case, the larger fraction of tail particles have protruded toward the aqueous phase (see Fig. 7), thereby the number of contacts between surfactant tails and nanotube surface decrease, leading to a weaker hydrophobic interactions between the SWNT and C_{16}TAB tails.

It is worthwhile to note that the number of C_{16}TAB adsorbed on the (5,7) SWNT at high surface coverage as well as on the (10,14) SWNT are bigger than those for C_{12}TAB molecules and therefore the effective surface charge of C_{16}TAB-coated nanotubes appears to be higher than C_{12}TAB-coated nanotubes. According to the Derjaguin–Landau–Verwey–Overbeek (DLVO) theory, the stability of a colloidal system is determined by the sum of electrostatic repulsive forces, associated with the double layer surrounding the colloid particle, and attractive van der Waals forces which exist between adjacent colloid particles [56, 57]. This theory suggests that a potential barrier resulting from the repulsive force prevents two particles approaching one another and adhering together. Therefore if the particles have a sufficiently high repulsion, the dispersion will resist coagulation and the colloidal system will be stable. The higher surface charge of C_{16}TAB-coated nanotubes produces a higher repulsive force between adjacent nanotubes which increases the potential barrier for aggregation of the nanotubes. It is this higher potential barrier that makes the C_{16}TAB-coated nanotubes more stable than C_{12}TAB-coated nanotubes against aggregation.

To study the influence of the SWNT diameter on the adsorption mechanism of C_{12}TAB and C_{16}TAB, we calculate the precise orientation of C_{12}TAB and C_{16}TAB molecules with respect to the SWNT axis according to Eq. 1. The orientation distribution for C_{12}TAB and C_{16}TAB surfactants with respect to the (5,7) and (10,14) SWNTs at low surface coverage are shown in Fig. 11. As can be observed in panel a Fig. 11, C_{12}TAB molecules prefer to orient almost parallel with respect to the axis of both SWNTs. The difference between C_{12}TAB adsorption on the (5,7) and (10,14) SWNTs is that due to a lower energetic cost for wrapping around a (10,14) nanotube, few C_{12}TAB molecules tend to wrap around the nanotube and form the wrapping angles which are significantly different from 0° or 180°. Thus, it seems that the SWNT diameter has no major effect on the orientation of the C_{12}TAB molecules and hence the random adsorption model can be reasonably used to describe the C_{12}TAB adsorption on a (10,14) SWNT. Consistent with the C_{12}TAB case, a careful inspection of the simulation snapshots along with the angle distribution profile of C_{16}TAB molecules demonstrates that the orientation of C_{16}TAB molecules is not influenced by the SWNT diameter. As shown in panel b Fig. 11, the angle distribution of C_{16}TAB molecules to the (10,14) SWNT shows two broad peaks at the same positions of those observed for the orientation of C_{16}TAB molecules to the (5,7) SWNT, indicating that some of the C_{16}TAB tails align with the nanotube axis and only their heads protrude toward the aqueous phase which form the angles close to 10° or 170°. On the other hand, due to a higher energetic cost for wrapping the C_{16}TAB molecules around the (10,14) SWNT, they do not have a tendency to warp around the nanotube. Instead, some of the C_{16}TAB molecules tend to form the contact angles which deviate considerably from 10° or 170°, identifying that not only the C_{16}TAB heads protrude toward the aqueous phase but also their tail particles stand up and rotate away from the (10,14) SWNT surface. It is likely that further increase of the SWNT diameter lead to some of the C_{16}TAB molecules to prefer to wrap around the SWNT. This

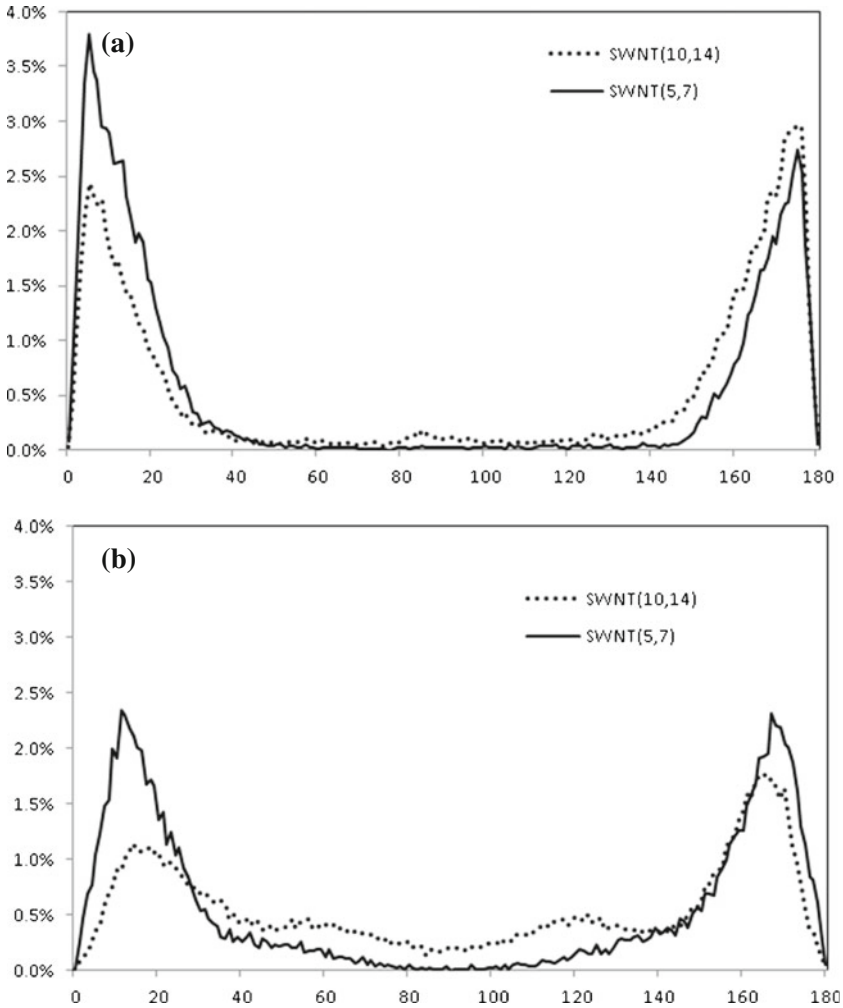

Fig. 11 Simulated distribution profiles of the angle formed between the vector of the surfactant and the SWNT axis at low surface coverage: **a** C_{12}TAB, and **b** C_{16}TAB

possibility should be examined in future work. It is worth pointing out that due to the larger number of the C_{16}TAB molecules present at the simulation box which make the hydrophobic interaction between C_{16}TAB tails stronger, the effective surface coverage for the C_{16}TAB adsorption on the (10,14) SWNT is larger than that observed for C_{16}TAB adsorption on the (5,7) SWNT, leading to the reduction in (10,14) SWNT surface area available per C_{16}TAB molecule. Thus, the orientation of C_{16}TAB molecules on a (10,14) SWNT is similar to that observed for the orientation of C_{16}TAB molecules on a (5,7) SWNT at high surface coverage and hence a cylindrical structure may be preferred for such a system.

In order to clarify the role of the SWNT diameter on the adsorption mechanism of C_{12}TAB and C_{16}TAB, we plot the radial distribution function (RDF) of both C_{12}TAB and C_{16}TAB tail and head segments with respect to the axis of the tube at low surface coverage. As shown in panel a Fig. 12, the tail segments RDF curve of C_{12}TAB surfactant display one strong peak which overlaps with the head segments RDF curve, indicating that the C_{12}TAB tails and heads are almost adsorbed at the same position on the SWNT surface. Only a small fraction of the C_{12}TAB heads are positioned farther away from the SWNT surface and extended toward the water, as can be seen from the shoulder found at around 1.6 nm. Therefore, this result also confirms that the random adsorption model can be acceptable for this system. For the C_{16}TAB adsorption, the RDF profile of tail segments shows an obvious peak which overlaps with the RDF of head segments, consistent with C_{12}TAB case. However, the peak intensity of the head segments RDF curve has been decreased. Instead, the shoulder intensity has been increased, confirming that the larger number of C_{16}TAB heads are extended far into the aqueous phase. Consequently, the C_{16}TAB aggregates adsorbed tend to form the cylindrical structure on the nanotube surface.

Conclusions

We have performed the large-scale all-atomistic MD simulation to probe the adsorption mechanism and morphology of aggregates of the cationic surfactants containing trimethylammonium headgroups (C_{12}TAB and C_{16}TAB), on the

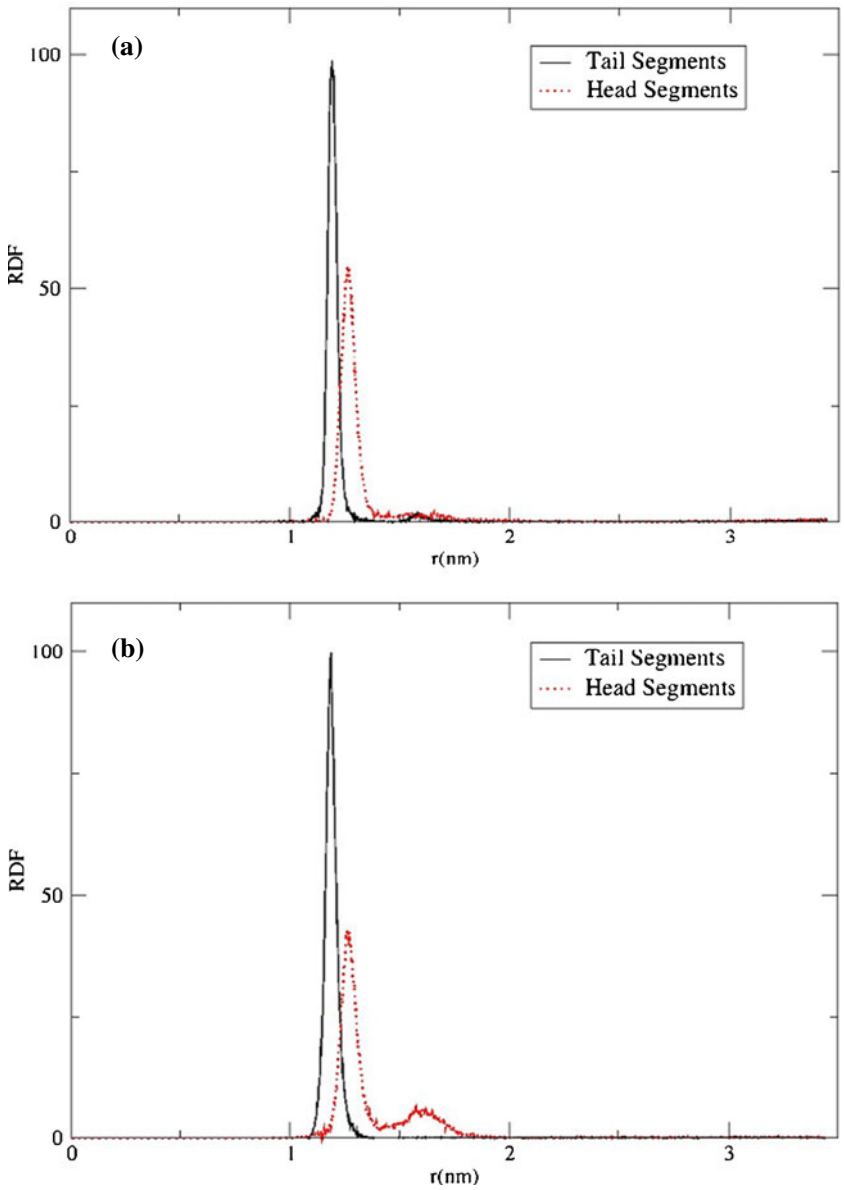

Fig. 12 Simulated radial distribution functions (RDFs) of surfactant tail and head segments around the CNT as a function of the distance from the axis of the tube **a** C_{12}TAB, and **b** C_{16}TAB at surface packing densities 1.05 molecule/nm^2

(5,7), and (10,14) SWNTs in aqueous solution. The effect of the surface coverage, length of the alkyl chain, and SWNT diameter has been investigated. The results have been quantified using representative simulation snapshots, radial distribution function profiles around the axis of the SWNT, and the distribution of the angles formed between the SWNT axis and the surfactant axis.

We have shown that at low surface coverage, both C_{12}TAB and C_{16}TAB tails prefer to align with the nanotube axis while their heads tend to position close to the SWNT surface. Of the commonly used models for surfactant adsorption onto SWNT, the random adsorption model most accurately describes this process. Upon increasing the C_{12}TAB surface coverage, the C_{12}TAB tails form a variety of wrapping angles to the SWNT axis and have a small tendency to orient perpendicular to the axis of the SWNT. For the C_{16}TAB surfactant at high surface coverage, the C_{16}TAB tails have rotated away from the nanotube surface, form various contact angles to the SWNT axis. Our results confirm that the cylinder-like structure can be preferable under high surface coverage for both surfactants. In addition, we have found that the hydrophobic interactions between surfactant tails contribute to the orientation of surfactant molecules on the SWNT surface, as well as the number of surfactant molecules adsorbed. Because of these interactions, the larger number of the C_{16}TAB molecules have been adsorbed onto both (5,7) and (10,14) SWNTs. Furthermore, based on the calculations for the effective potential of mean force between carbon nanotubes in aqueous surfactant systems available in the literature, it appears that the C_{16}TAB surfactant is able to stabilize SWNT suspensions more effectively than the C_{12}TAB surfactant. Our findings reported in this study, shed some light on the adsorption mechanism of

cationic surfactants on the SWNT surface as well as the role of the tail length on the adsorption process which may guild future research on the enhancement of the dispersion stability of individual SWNTs in aqueous solution.

References

1. Saito R, Dresselhaus G, Dresselhaus MS (1998) Physical properties of carbon nanotubes. Imperial College Press, London
2. Baughman RH, Zakhidov AA, de Heer WA (2002) Carbon nanotubes-the route toward applications. Science 297:787–792
3. Wang H, Zhou W, Ho DL, Winey KI, Fischer JE, Glinka CJ, Hobbie EK (2004) Dispersing single-walled carbon nanotubes with surfactants: a small angle neutron scattering Study. Nano Lett 4:1789–1793
4. Clark MD, Subramanian S, Krishnamoorti R (2011) Understanding surfactant aided aqueous dispersion of multi-walled carbon nanotubes. J Colloid Interface Sci 354:144–151
5. Chen J, Hamon MA, Hu H, Chen Y, Rao AM, Eklund PC, Haddon RC (1998) Solution properties of single-walled carbon nanotubes. Science 282:95–98
6. Mickelson ET, Chiang IW, Zimmerman JL, Boul PJ, Lozano J, Liu J, Smalley RE, Hauge RH, Margrave JL (1999) Solvation of fluorinated single-wall carbon nanotubes in alcohol solvents. J Phys Chem B 103:4318–4322
7. Qin YJ, Shi JH, Wu W, Li XL, Guo ZX, Zhu DB (2003) Concise route to functionalized carbon nanotubes. J Phys Chem B 107:12899–12901
8. Georgakilas V, Tagmatarchis N, Pantarotto D, Bianco A, Briand JP, Prato M (2002) Amino acid functionalisation of water soluble carbon nanotubes. Chem Commun 24:3050–3051
9. Wang Q, Han Y, Wang Y, Qin Y, Guo Z (2008) Effect of surfactant structure on the stability of carbon nanotubes in aqueous solution. J Phys Chem B 112:7227–7233
10. Dwyer C, Guthold M, Falvo M, Washburn S, Superfine R, Erie D (2002) DNA-functionalized single-walled carbon nanotubes. Nanotechnology 13:601–604
11. Liu J, Rinzler AG, Dai H, Hafner JH, Bradley RK, Boul PJ, Lu A, Iverson T, Shelimov K, Huffman CB, Rodriguez-Macias F, Shon YS, Lee TR, Colbert DT, Smalley RE (1998) Fullerene pipes. Science 280:1253–1256
12. Hudson JL, Casavant MJ, Tour JM (2004) Water-soluble, exfoliated, nonroping single-wall carbon nanotubes. J Am Chem Soc 126:11158–11159
13. Dong B, Su Y, Liu Y, Yuan J, Xu J, Zheng L (2011) Dispersion of carbon nanotubes by carbazole-tailed amphiphilic imidazolium ionic liquids in aqueous solutions. J Colloid Interface Sci 356:190–195
14. Zhao YL, Stoddart JF (2009) Noncovalent functionalization of single-walled carbon nanotubes. Acc Chem Res 42:1161–1171
15. Zhang XF, Liu T, Sreekumar TV, Kumar S, Moore VC, Haug RH, Smalley RE (2003) Poly(vinyl alcohol)/SWNT composite film. Nano Lett 3:1285–1288
16. Kang YK, Lee O-S, Deria P, Kim SH, Park T-H, Bonnell DA, Saven JG, Therien MJ (2009) Helical wrapping of single-walled carbon nanotubes by water soluble poly(p-phenyleneethynylene). Nano Lett 9:1414–1418
17. Blanch AJ, Lenehan CE, Quinton JS (2010) Optimizing surfactant concentrations for dispersion of single-walled carbon nanotubes in aqueous solution. J Phys Chem B 114:9805–9811
18. Islam MF, Rojas E, Bergey DM, Johnson AT, Yodh AG (2003) High weight fraction surfactant solubilization of single-wall carbon nanotubes in water. Nano Lett 3:269–273
19. Tan Y, Resasco DE (2005) Dispersion of single-walled carbon nanotubes of narrow diameter distribution. J Phys Chem B 109:14454–14460
20. Kim HS, Park WI, Kang M, Jin HJ (2008) Multiple light scattering measurement and stability analysis of aqueous carbon nanotube dispersions. J Phys Chem Solids 69:1209–1212
21. Kiraly Z, Findenegg GH, Mastalir A (2003) Chain-length anomaly in the two-dimensional ordering of the cationic surfactants CnTAB at the graphite/water interface, revealed by advanced calorimetric methods. J Phys Chem B 107:12492–12496
22. Angelikopoulos P, Bock H (2010) The differences in surfactant adsorption on carbon nanotubes and their bundles. Langmuir 26:899–907
23. Matarredona O, Rhoads H, Li ZR, Harwell JH, Balzano L, Resasco DE (2003) Dispersion of single-walled carbon nanotubes in aqueous solutions of the anionic surfactant NaDDBS. J Phys Chem B 107:13357–13367
24. Wu Y, Hudson JS, Lu Q, Moore JM, Mount AS, Rao AM, Alexov E, Ke PC (2006) Coating single-walled carbon nanotubes with phospholipids. J Phys Chem B 110:2475–2478
25. Yurekli K, Mitchell CA, Krishnamoorti R (2004) Small-angle neutron scattering from surfactant-assisted aqueous dispersions of carbon nanotubes. J Am Chem Soc 126:9902–9903
26. Wallace EJ, Sansom MSP (2007) Carbon nanotube/detergent interactions via coarse-grained molecular dynamics. Nano Lett 7:1923–1928
27. Tummala NR, Striolo A (2009) SDS surfactants on carbon nanotubes: aggregate morphology. ACS Nano 3:595–602
28. Xu ZJ, Yang XN, Yang Z (2010) A molecular simulation probing of structure and interaction for supramolecular sodium dodecyl sulfate/single-wall carbon nanotube assemblies. Nano Lett 10:985–991
29. Lin S, Blankschtein D (2010) Role of the bile salt surfactant sodium cholate in enhancing the aqueous dispersion stability of single-walled carbon nanotubes: a molecular dynamics simulation study. J Phys Chem B 114:15616–15625
30. Tummala NR, Morrow BH, Resasco DE, Striolo A (2010) Stabilization of aqueous carbon nanotube dispersions using surfactants: insights from molecular dynamics simulations. ACS Nano 4:7193–7204
31. Suttipong M, Tummala NR, Kitiyanan B, Striolo A (2011) Role of surfactant molecular structure on self-assembly: aqueous SDBS on carbon nanotubes. J Phys Chem C 115:17286–17296
32. Hess B, Kutzner C, van der Spoel D, Lindahl E (2008) GROMACS 4: algorithms for highly efficient, load-balanced, and scalable molecular simulation. J Chem Theory Comput 4:435–447
33. Jorgensen WL, Maxwell DS, Tirado-Rives J (1996) Development and testing of the OPLS all-atom force field on conformational energetics and properties of organic liquids. J Am Chem Soc 118:11225–11236
34. Berendsen HJC, Grigera JR, Straatsma TP (1987) The missing term in effective pair potentials. J Phys Chem 91:6269–6271
35. Miyamoto S, Kollman PA (1992) Settle: an analytical version of the SHAKE and RATTLE algorithm for rigid water models. J Comput Chem 13:952–962
36. Vanquelef E, Simon S, Marquant G, Garcia E, Klimerak G, Delepine JC, Cieplak P, Dupradeau F-Y (2011) R.E.D. Server: a web service for deriving RESP and ESP charges and building force field libraries for new molecules and molecular fragments. Nucl Acids Res 39:W511–W517
37. Dupradeau F-Y, Pigache A, Zaffran T, Savineau C, Lelong R, Grivel N, Lelong D, Rosanski W, Cieplak P (2010) The R.E.D. tools: advances in RESP and ESP charge derivation and force field library building. Phys Chem Chem Phys 12:7821–7839
38. Bayly CI, Cieplak P, Cornel W, Kollman PA (1993) A well-behaved electrostatic potential based method using charge restraints for deriving atomic charges: the RESP model. J Phys Chem 97:10269–10280
39. Schmidt MW, Baldridge KK, Boatz JA, Elbert ST, Gordon MS, Jensen JH, Koseki S, Matsunaga N, Nguyen KA, Su S, Windus

TL, Dupuis M, Montgomery JA (1993) General atomic and molecular electronic structure system. J Comput Chem 14:1347–1363
40. Hess B, Bekker H, Berendsen HJC, Fraaije JGEM (1997) LINCS: a linear constraint solver for molecular simulations. J Comput Chem 18:1463–1472
41. Darden T, York D, Pedersen L (1993) Particle mesh Ewald: an N-log(N) method for Ewald sums in large systems. J Chem Phys 98:10089–10092
42. Essmann U, Perera L, Berkowitz ML, Darden T, Lee H, Pedersen LG (1995) A smooth particle mesh Ewald method. J Chem Phys 103:8577–8592
43. Hockney RW, Goel SP, Eastwood JW (1974) Quiet high resolution computer models of a plasma. J Comput Phys 14:148–158
44. Verlet L (1967) Computer experiments on classical fluids. I. Thermodynamical properties of Lennard-Jones molecules. Phys Rev 159:98–103
45. Bussi G, Donadio D, Parrinello M (2007) Canonical sampling through velocity rescaling. J Chem Phys 126:014101-1–014101-7
46. Parrinello M, Rahman AR (1981) Polymorphic transitions in single crystals: a new molecular dynamics method. J Appl Phys 52:7182–7190
47. Leach AR (2001) Molecular modelling: principles and applications, 2nd edn. Prentice Hall, Harlow, England
48. Humphrey W, Dalke A, Schulten K (1996) VMD - visual molecular dynamics. J Mol Graph 14:33–38
49. Qi X, Ping-Hua W, Ling-Ling J, Xiao-Ke T, Lin-Li O (2007) Dispersion of carbon nanotubes in aqueous solution with cationic surfactant CTAB. J Inorg Mater 22:1122–1126
50. Manning GS (1979) Counterion binding in polyelectrolyte theory. Acc Chem Res 12:443–449
51. Manning GS (1969) Limiting laws and counterion condensation in polyelectrolyte solutions I. Colligative properties. J Chem Phys 51:924–933
52. Manning GS (2007) Counterion condensation on charged spheres, cylinders, and planes. J Phys Chem B 111:8554–8559
53. Bandyopadhyay S, Shelley JC, Tarek M, Moore PB, Klein ML (1998) Surfactant aggregation at a hydrophobic surface. J Phys Chem B 102:6318–6322
54. Manne S, Cleveland JP, Gaub HE, Stucky GD, Hansma PK (1994) Direct visualization of surfactant hemimicelles by force microscopy of the electrical double layer. Langmuir 10:4409–4413
55. Manne S, Gaub HE (1995) Molecular organization of surfactants at solid–liquid interfaces. Science 70:1480–1483
56. Derjaguin B, Landau L (1941) Theory of the stability of strongly charged lyophobic sols and of the adhesion of strongly charged particles in solutions of electrolytes Acta Physicochim. URSS 14:633–662
57. Verwey EJW, Overbeek JTG (1948) Theory of the stability of lyophobic colloids. Elsevier, Amsterdam